

Optical Emissions from Proton Aurora

D. Lummerzheim¹, M. Galand², and M. Kubota³

¹Geophysical Institute, University of Alaska, Fairbanks, Alaska

²Center for Space Physics, Boston University, Boston, Massachusetts

³Communications Research Laboratory, Tokyo, Japan

Received: x.x.2001 – Accepted: x.x.2002

Abstract.

Hydrogen emissions are the signature of proton aurora. The Doppler-shifted hydrogen emission lines can be interpreted in terms of the mean energy of the precipitating protons. A red shifted component of the line profiles observed from the ground indicates upward going hydrogen atoms due to angular redistribution of the precipitation. Secondary electrons from ionization and stripping collisions also contribute to the auroral emissions. Since the energy distribution of these secondaries has a lower mean energy than secondary electrons in electron aurora, the relative brightness of emission features differs from that in electron aurora. The secondaries contribute little to additional ionization. These differences between proton and electron aurora can lead to misinterpretation when brightness ratios are used to derive ionospheric conductances with parameterizations that are based on electron aurora.

1 Introduction

Aurora that is caused by proton precipitation is not as bright and spectacular as that caused by electrons. This does not, however, indicate that the effect of proton aurora on the ionosphere is negligible. Precipitating protons easily charge exchange in collisions with ambient neutral oxygen. The resulting hydrogen atom still has most of the initial energy of the original proton, but is not bound by the geomagnetic field anymore. It maintains the direction of the pitch angle of the spiraling proton, and causes the energetic particles to spread out horizontally. The auroral emissions are therefore a diffuse glow which is spread out over a large part of the sky.

In the process of penetrating the upper atmosphere, the incident proton beam and the resulting mixture of energetic protons and hydrogen atoms causes ionization, dissociation, and excitation. The energy of the incident protons is used up by these processes and by energizing secondary electrons in

ionization collisions. These secondary electrons have an energy distribution with a lower typical energy than secondary electrons in photoionization or ionization by incident auroral electrons. The proton aurora secondary electrons contribute to excitation of ambient neutrals, and lead to a significant fraction of the optical emissions. Emissions also result from impact of proton or hydrogen on ambient neutrals, as well as from the energetic hydrogen atoms themselves.

2 Observations of Hydrogen Emission Lines

The brightest of the Doppler-shifted hydrogen lines, a unique signature of proton precipitation, is the Lyman α line in the extreme UV. This emission is suitable for satellite observations, but has to be separated from the geocorona. The geocorona is scattered sunlight, and is not Doppler-shifted. The auroral emissions can therefore be separated from the geocorona by high resolution spectroscopic observations, as it is done on the IMAGE satellite (Mende et al., 2000a,b), or the featureless and smoothly varying geocorona can be spatially interpolated across the auroral oval and then subtracted to obtain the auroral emissions (Galand et al., 2001).

Two hydrogen lines in the visible are the Balmer H_α and H_β lines at 656.3 nm and 486.1 nm. The H_α sits in close proximity of the N_2 1P bands, which are bright in electron aurora. Separating the H_α line from the N_2 1P bands requires good spectral resolution. The H_β line does not have distinct emissions from electron aurora in its immediate spectral surrounding. However, the spectral region around H_β shows a background continuum brightness that varies with the distinct electron auroral emissions. This background is of the same brightness as the line itself. For observations of the H_β brightness it is therefore necessary to subtract the background brightness. This can be done by obtaining the background and line brightness by tilting filter photometers (Valance Jones et al., 1982; Lummerzheim et al., 1990; Deehr and Lummerzheim, 2001) or with a spectrometer which has sufficient spectral range to cover the emission line and some

Correspondence to: D. Lummerzheim

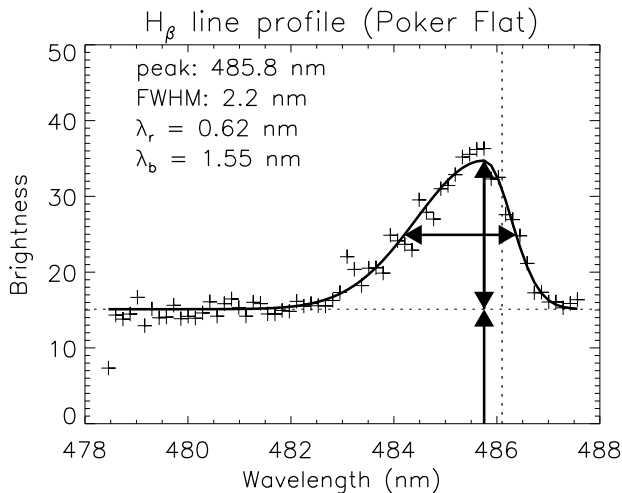


Fig. 1. H_{β} line profile from zenith observations. The crosses are the observations, the solid line is a fit to the data. The rest wavelength of 486.1 nm is indicated by the vertical dotted line. The arrows indicate the parameters that are used in the fit. The obtained peak wavelength and the half widths of the line towards shorter (λ_b) and longer (λ_r) wavelengths from the peak position are shown (from Lummerzheim and Galand (2001)).

of the surrounding background (Lummerzheim and Galand, 2001; Lanchester et al., this issue). Fig. 1 shows an example of the H_{β} line profile from magnetic zenith observations in Poker Flat, Alaska. This spectrum was obtained with a Fastie-Ebert 1m spectrometer at 0.4 nm spectral resolution. The spectrum shows the constant background, the shifted peak of the emission, and the asymmetric line profile.

All-sky imaging of proton aurora using the H_{β} line is difficult because of the varying background. The Communication Research Laboratory (CRL) of Japan has two all-sky imagers installed at Poker Flat, Alaska. Both cameras have telecentric lens systems and cycle through different filters. They are operated such that an H_{β} image and an image of the background brightness in the spectral vicinity of H_{β} are taken simultaneously. The filters used are interference filters with high rejection outside the passband to avoid contamination by other auroral emissions. The H_{β} filter is centered at 485.75 nm with a full width at half maximum (FWHM) of 1.7 nm, while the background filter is centered at 481.25 nm with a FWHM of 1.7 nm. The background filter is far enough from the H_{β} line that the blue shifted wing of the Doppler profile does not contribute (compare to Fig. 1). An example of the images from these cameras is shown in Fig. 2. The images are calibrated and are displayed in a linear grey scale. The background image has similar features as the image of OI(557.7 nm), which was taken 30 s before the H_{β} image. Note the stars that are visible in the background image, e.g. the big dipper is near the top of the image. The bright speck in the lower left that remains even in the final image after stars have been removed is Jupiter. The image of the proton aurora on the bottom right was obtained from the difference of the H_{β} and the background image. Additionally, stars were removed and the images were corrected for the

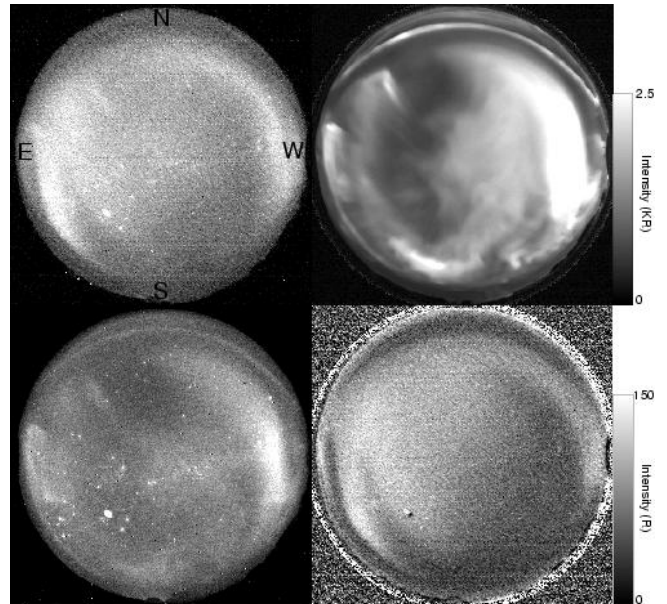


Fig. 2. All sky images from the CRL imager at Poker Flat, Alaska, taken at 10:30 UT on 6 Nov, 2000. The orientation of the images has north at the top, and west to the right. The top left image is from the H_{β} filter, below that is the simultaneous background image. Top right is a OI(557.7) image taken 30 s prior to the H_{β} image. Bottom right is the difference of the H_{β} and background image. Exposure for the H_{β} and background image is 45 s, and 3 s for the green line image. The grey scale for the OI(557.7) image covers 2.5 kR, and 150 R for the H_{β} image

van Rhijn effect and atmospheric extinction.

These images demonstrate the importance of background removal from H_{β} observations. Not all bright areas in the original H_{β} image are due to proton precipitation. This particular image also shows that electron aurora, which is represented by the OI(557.7 nm) image, and proton aurora can be quite intermingled, and are not necessary separated into north-south regions.

3 Modeling of Emissions in Proton Aurora

Given a neutral atmospheric model, cross sections for collision processes, and the energy and pitch angle distribution of the incident proton beam, the altitude and energy distribution of the proton and hydrogen atom flux can be calculated from the solution of a coupled H/H⁺ transport equation. A number of techniques have been developed to solve these coupled equations: Monte-Carlo simulations (Kozelov and Ivanov, 1992; Decker et al., 1996; Lorentzen et al., 1998; Synnes et al., 1998; Gerard et al., 2000), quasi-analytical approaches (Jasperse and Basu, 1982; Basu et al., 1987), and explicit solutions (Basu et al., 1993; Strickland et al., 1993; Galand et al., 1997, 1998). From the solution of the coupled H/H⁺ transport equations one can determine the altitude distribution of the secondary electron source. These serve as input to an electron transport calculation. Auroral emissions can be calculated from the altitude and energy distribution of the proton, hydrogen atoms, and electron fluxes. The secondary

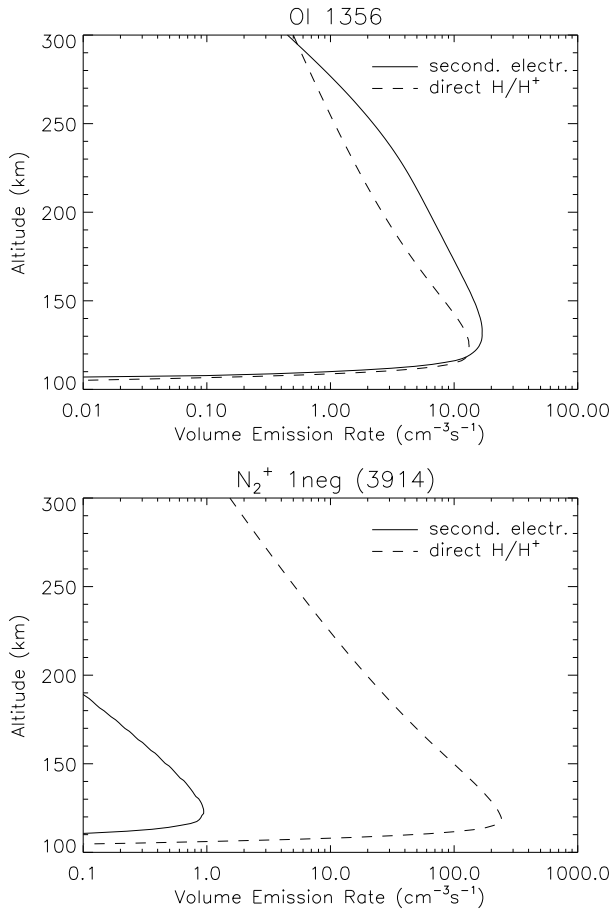


Fig. 3. Volume emission rate profiles for OI(135.6 nm) and N_2^+ 1N (391.4 nm) from proton precipitation with a mean energy of 15 keV and an energy flux of 1 mW m^{-2} . The contribution to the emission by secondary electrons (solid line) is comparable to the direct excitation by the H/H^+ (dashed line) for the OI line, while negligible for the N_2^+ 1N band.

electrons have a lower mean energy than the secondary electrons in electron aurora, and contribute very little to additional ionization, and to optical emissions that result from excited states with a high energy threshold. Emissions from states with a low excitation potential, like the OI(630.0 nm) red line, on the other hand, are mostly due to excitation by the secondary electrons, and are strong in proton aurora (Lummerzheim et al., 2001). In the case of the red line, the dominance of the secondary electrons in the excitation process is further strengthened by quantum mechanical selection rules. The excitation of $O(^1D)$ by proton impact requires a spin exchange which is highly unlikely, so that only the hydrogen atoms and the secondary electrons can excite the state.

The relative contribution to emissions from direct impact of the H/H^+ and from excitation by the secondary electrons is demonstrated in Fig. 3 which shows altitude profiles of the emission of OI(135.6 nm) with an excitation threshold of 9.15 eV and the emission of the N_2^+ 1N (391.4 nm) with a threshold of 18.75 eV. For the OI emission, the excitation by secondary electrons is larger than the direct excitation by the H/H^+ beam, while the first negative emission is dominated

by the H/H^+ ionization impact on N_2 .

4 Doppler-Shifted Hydrogen Emissions

Hydrogen emissions occur only in proton aurora. Ambient hydrogen densities in the upper atmosphere, where particles deposit most of their energy, are too small to lead to any observable emission by excitation in electron aurora. In proton aurora precipitating protons undergo charge exchange collisions with atomic oxygen. The resulting hydrogen atoms subsequently get excited in collisions with the atmospheric constituents and radiate with the hydrogen spectral lines. Because the hydrogen atom retains most of the kinetic energy of the incident proton, the emissions are Doppler-shifted. For observations perpendicular to the magnetic field, the gyroscopic motion of the protons determines the velocity component for the Doppler shift. The resulting line profile is symmetric around the rest wavelength, and the width of the line depends on the energy distribution of the precipitating particles. For observations in the magnetic zenith, the field aligned velocity component is responsible for the Doppler shift, and the line is asymmetrical and shifted towards the blue, as most of the energetic particles are going downward.

The precipitating H/H^+ stream loses most of its energy and makes most of the excitation and ionization in the lower thermosphere. Depending on the energy of the incident protons, most emissions come from altitudes in the 100-150 km range. The Doppler profile of the hydrogen lines is thus not just representative of the energy distribution of the incident proton flux, but of the energy distribution of the particles after they have penetrated the thermosphere and undergone a number of collisions. At this altitude the incident beam has experienced energy and angular redistribution. For magnetic zenith observations the position of the peak of the line profile is dependent on the product of the energy dependent cross section for excitation, and the hydrogen atom distribution function after it has undergone energy and angular redistribution. Lummerzheim and Galand (2001) have shown that the position of the peak of the Doppler line profile of the H_β emission at 486.1 nm shows less variation over the course of a night than the width of the line. Model calculations (Galand et al., 1998) support the interpretation that increasing the energy of precipitating protons has a stronger effect on raising the blue wing of the line than on the position of the peak. In order to compare model results to measured line profiles, it is important to convolve the model results with an instrumental function. The line profile is asymmetric, and a low resolution spectrometer will measure a line profile that peaks at a shorter wavelength than a high resolution instrument. When high energy proton precipitation raises the blue wing of the line profile, this would also translate into a motion of the measured line profile peak towards shorter wavelengths.

Another consequence of the energy and angular redistribution of the incident beam is that part of the energetic hydrogen atoms are moving upward in the lower thermosphere. The model by Galand et al. (1998) predicts that a red shifted

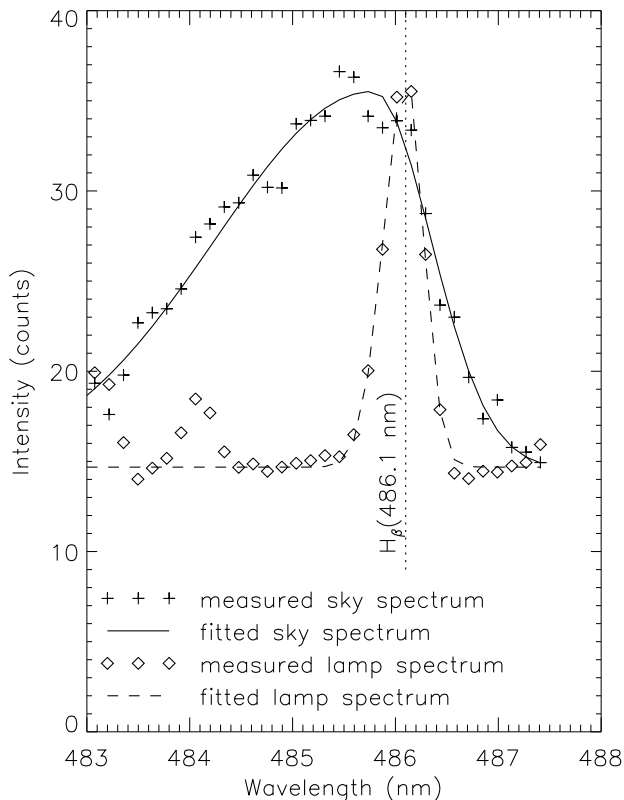


Fig. 4. Observed and fitted line profiles from the aurora and from a calibration lamp. The H_{β} line shape of the lamp spectrum shows the instrument spectral resolution. The red wing of the auroral spectrum extends well past the unshifted H_{β} wavelength, and past the red wing of the lamp's profile. This is a clear indication that the red wing of the auroral line profile is due to upward moving hydrogen atoms (from Lummerzheim and Galand (2001)).

wing of the Doppler profile should be detectable with spectroscopic observations at high enough resolution. An example is shown by Lummerzheim and Galand (2001), and reproduced here in Fig. 4. The high spectral resolution observations on Svalbard reported by Lanchester et al. (this issue) also show a significant red wing in the H_{β} line profile. Magnetic mirroring only plays a minor role in producing the red shifted emission, although it may contribute to upward moving protons and hydrogen (Eather, 1966; Kozelov, 1993; Galand and Richmond, 1999). Mirroring is most effective in producing upward moving protons at high altitudes. Emissions, however, result from lower altitudes, where scattering through collisions rather than mirroring determine the angular distribution of the precipitation.

5 Emissions from H/H^+ and Secondary Electron Impact

The secondary electrons in proton aurora cause the same excitation and emission as those observed in electron aurora. The difference only comes from the differences in the energy distribution of the secondary electrons. Hydrogen atom

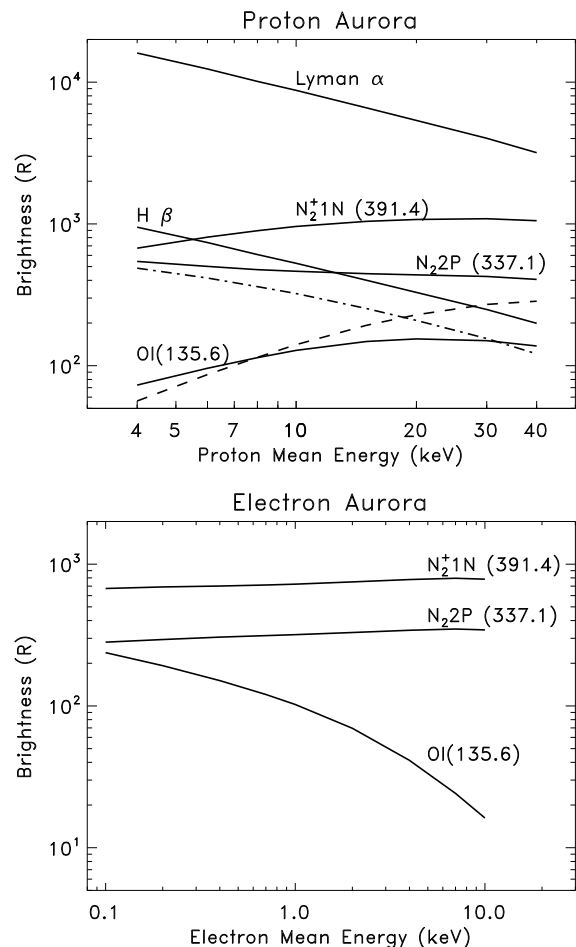


Fig. 5. Column integrated emission rates in proton and electron aurora as a function of mean energy of the incident particle precipitation. An energy flux of 1 mW m^{-2} was assumed in all cases. For the N_2 2P emission, the contribution of direct H/H^+ impact (dash-dotted) and secondary electron impact (dashed) on N_2 are shown separately (top panel).

and proton impact on the neutral constituents of the thermosphere also causes emissions of the full auroral spectrum. Fig. 5 shows the column integrated emission rate of some selected auroral emission features, neglecting atmospheric extinction. All calculations assumed a Maxwellian energy distribution with an energy flux of 1 mW m^{-2} and varying mean energy. In the case of the proton aurora, almost all of the N_2^+ 1N emission is due to direct H/H^+ impact on N_2 , while for $\text{OI}(135.6 \text{ nm})$ most of the emission results from the secondary electrons. The contributions to the emission of the N_2 2P bands from H/H^+ and secondary electrons are shown separately. Direct excitation dominates at low energies, secondary electron excitation dominates at high energies. The electron impact excitation cross section for the $\text{N}_2(\text{C}^3\Pi)$ state peaks at low energy, thus the secondary electrons, mainly produced in hard proton aurora, are very effective for this excitation. In soft proton precipitation, incident protons are less efficient to ionize and the contribution to $\text{N}_2(\text{C}^3\Pi)$ is dominated by direct impact. In electron aurora the distinction between excitation from primary and secondary electrons is meaningless. The low energy part of the precipitating electrons, which arises from secondary production as well as energy degradation is independent of the mean energy of the incident fluxes. The total excitation from all impact processes of $\text{N}_2(\text{C}^3\Pi)$ yields a constant column emission rate.

6 Summary and Conclusion

The profile of the Doppler-shifted hydrogen emissions in proton aurora depends on the energy distribution of the incident particles. For ground based observations, an elevated blue wing of the line profile signals high energy precipitation. Depending on the spectral resolution of the observation, the increase in brightness at shorter wavelengths can also lead to a repositioning of the peak of the line profile to shorter wavelengths. A red shifted wing of the Doppler profile indicates upward moving hydrogen atoms from angular redistribution in collisional process. Angular redistribution occurs in elastic as well as in inelastic collisions.

Secondary electrons cause additional auroral emissions. Because of their low energy, these secondaries contribute very little to additional ionization. The ratio of different emissions in electron aurora can be used to obtain the energy and energy flux of the precipitating electrons, and subsequently the ionization rate profile. Ionospheric parameters like conductances can then be derived and put into direct relation to specific auroral brightnesses. In proton aurora, the brightness ratio between emission features has a different dependence on the energy flux and mean energy of the precipitating particles, compared to the electron aurora. In particular, the ionization rate that would be derived from brightness and brightness ratios in proton aurora is different from that in electron aurora. This leads to misinterpretation of ionospheric parameters like the conductance, if the brightness ratios are interpreted without knowledge of the type of particle precipitation.

Acknowledgements. Funding for this research was provided by the NASA ISTP/GGS theory program, grant NAG5-7683. MG was supported by NSF grant ATM-0003175.

References

- Basu, B., Jasperse, J. R., Robinson, R. M., Vondrak, R. R., and Evans, D. S., Linear transport theory of auroral proton precipitation: A comparison with observations, *J. Geophys. Res.*, **92**, 5920, 1987.
- Basu, B., Jasperse, J. R., Strickland, D. J., and Jr., R. E. D., Transport-theoretic model for the electron-proton-hydrogen atom aurora, 1 Theory, *J. Geophys. Res.*, **98**, 21,517, 1993.
- Decker, D. T., Kozelov, B. V., Basu, B., Jasperse, J. R., and Ivanov, V. E., Collisional degradation of the proton-H atom fluxes in the atmosphere: A comparison of theoretical techniques, *J. Geophys. Res.*, **101**, 26,947, 1996.
- Deehr, C. S. and Lummerzheim, D., Ground-based optical observations of hydrogen emission in the auroral substorm, *J. Geophys. Res.*, **106**, 33–44, 2001.
- Eather, R. H., Red shift of auroral hydrogen profiles, *J. Geophys. Res.*, **71**, 5027, 1966.
- Galand, M. and Richmond, A. D., Magnetic mirroring in an incident proton beam, *J. Geophys. Res.*, **104**, 4447–4456, 1999.
- Galand, M., Lilensten, J., Kofman, W., and Sidje, R. B., Proton transport model in the ionosphere 1. Multistream approach of the transport equations, *J. Geophys. Res.*, **102**, 22 261–22 272, 1997.
- Galand, M., Lilensten, J., Kofman, W., and Lummerzheim, D., Proton transport model in the ionosphere. 2. Influence of magnetic mirroring and collisions on the angular redistribution in a proton beam, *Annales Geophysicae*, **16**, 1308, 1998.
- Galand, M., Lummerzheim, D., Stephan, A. W., Bush, B. C., and Chakrabarti, S., Electron and proton aurora observed spectroscopically in the far ultraviolet, *J. Geophys. Res.*, p. submitted, 2001.
- Gerard, J.-C., Hubert, B., Bisikalo, D. V., and Shematovich, V. I., A model of the Lyman- α line profile in the proton aurora, *J. Geophys. Res.*, **105**, 15,795, 2000.
- Jasperse, J. R. and Basu, B., Transport theoretic solutions for auroral proton and H atom fluxes and related quantities, *J. Geophys. Res.*, **87**, 811, 1982.
- Kozelov, B. V., Influence of the dipolar magnetic field on transport of proton-H atom fluxes in the atmosphere, *Ann. Geophys.*, **11**, 697, 1993.
- Kozelov, B. V. and Ivanov, V. E., Monte-Carlo calculation of proton-hydrogen atom transport in N_2 , *Planet. Space Sci.*, **40**, 1503, 1992.
- Lanchester, B. S., Lummerzheim, D., Rees, M. H., Galand, M., Baumgardner, J., and Rich, F., Proton and electron precipitation over Svalbard – first results from a new imaging spectrograph (HiTIES), this issue.
- Lorentzen, D. A., Sigernes, F., and Deehr, C. S., Modeling and observations of dayside auroral hydrogen emission Doppler profiles, *J. Geophys. Res.*, **103**, 17,479, 1998.
- Lummerzheim, D. and Galand, M., The profile of the hydrogen H_β emission line in proton aurora, *J. Geophys. Res.*, **106**, 23–32, 2001.
- Lummerzheim, D., Rees, M. H., and Romick, G. J., The application of spectroscopic studies of the aurora to thermospheric neutral composition, *Planet. Space Sci.*, **38**, 67–78, 1990.
- Lummerzheim, D., Galand, M., Semeter, J., Mendillo, M. J., Rees, M. H., and Rich, F. J., Emission of O I(630 nm) in proton aurora, *J. Geophys. Res.*, **106**, 141–148, 2001.
- Mende, S. B., Heeterds, H., Frey, H. U., Lampton, M., Geller, S. P., Habraken, S., Renotte, E., Jamar, C., Rochus, P., Spann, J., Fuselier, S. A., Gerard, J.-C., Gladstone, R., Murphree, S., and Cogger, L., Far ultraviolet imaging from the IMAGE spacecraft: 1. System design, *Space Science Reviews*, **91**, 243–270, 2000a.
- Mende, S. B., Heeterds, H., Frey, H. U., Stock, J. M., Lampton, M., Geller, S. P., Abiad, R., Siegmund, O. H. W., Habraken, S., Renotte, E., Jamar, C., Rochus, P., Gerard, J.-C., Sigler, R., and Lauche, H., Far ultraviolet imaging from the IMAGE spacecraft: 3. Spectral imaging of Lyman- α ; and OI 135.6 nm, *Space Science Reviews*, **91**, 287–318, 2000b.

Strickland, D. J., Daniell Jr., R. E., Jasperse, J. R., and Basu, B., Transport-theoretic model for the electron-proton-hydrogen atom aurora, 2 Model results, *J. Geophys. Res.*, *98*, 21 533, 1993.

Synnes, S. A., raas, F. S., and Hansen, J. P., Monte-Carlo simulation of proton aurora, *J. Atmos. Sol. Terr. Phys.*, *60*, 1695, 1998.

Vallance Jones, A., Creutzberg, F., Gattinger, R. L., and Harris, F. R., Auroral studies with a chain of meridian-scanning photometers. I - Observations of proton and electron aurora in magnetospheric substorms, *J. Geophys. Res.*, *87*, 4489–4503, 1982.